ESI: Structural behaviour of sodium hyaluronate in concentrated oppositely charged surfactant solution†

Philipp Buchold Ralf Schweins Michael Gradzielski

January 26, 2017

1 Two phase region

Precipitates of polyelectrolyte and surfactants can vary widely in their appearance. The system HA/TTAB in aqueous NaBr solution shows strong dependence on NaBr addition, as to be expected. Fig. S1 shows the swelling of the precipitate with increasing NaBr concentration of one fixed mixing ratio close to the phase boundary.

This swelling is even more obvious for samples far away from the phase boundary as seen in Fig. S2.

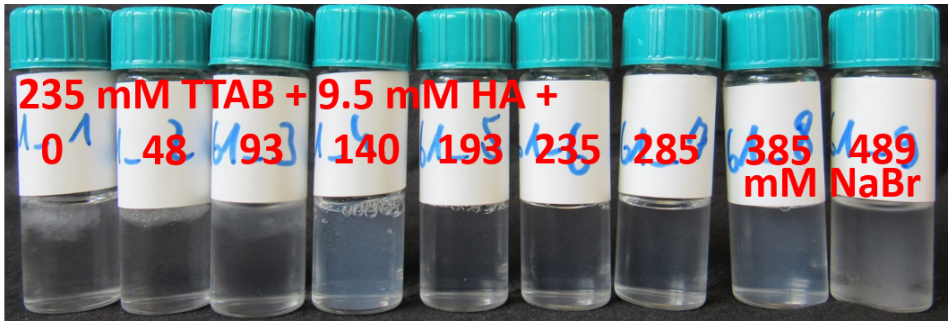

Fig. S 1 HA/TTAB complexes near the phase boundary with various amounts of NaBr.

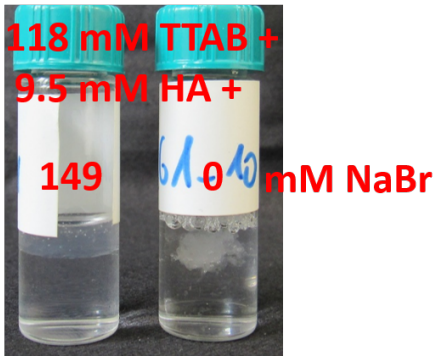

Fig. S 2 HA/TTAB complexes further away from the phase boundary with various amounts of NaBr.

2 Phase Behaviour with Other Polyelectrolytes

The direct comparison to other PESCs was also documented.

In Fig. S 3 different mixtures of polystyrenesulfonate with TTAB in 160 mM NaBr in D_2O showing fine dust like precipitation at low TTAB as clumpy cloudy at higher TTAB concentration. Similar to that is the sodium poly(methacrylate) PMA/TTAB precipitate shown in Fig. S4. The dust like solid phase sediments after one day at rest, but can be re-dispersed via simply shaking. The mixture with poly(acrylicacid), PAA, gives a milky white solution (Fig. S5).

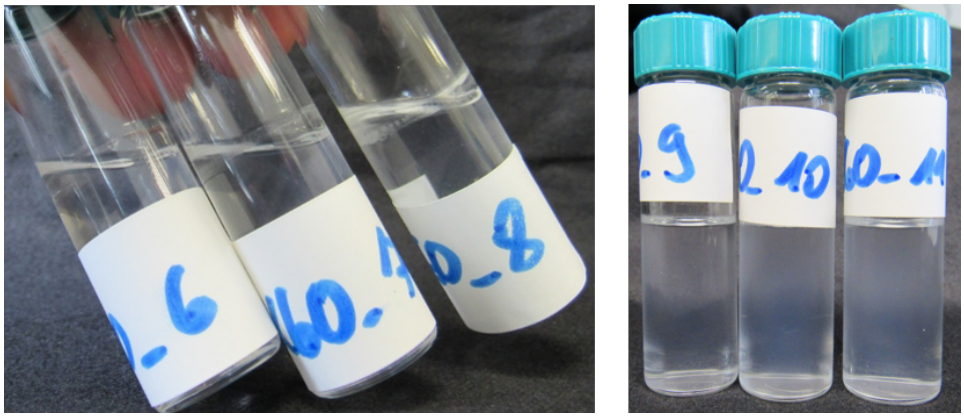

Fig. S 3 PSS/TTAB complexes. (From left: 245 mM TTAB + 1/2/4 mM PSS, 496 mM TTAB + 1/4/5 mM PSS.

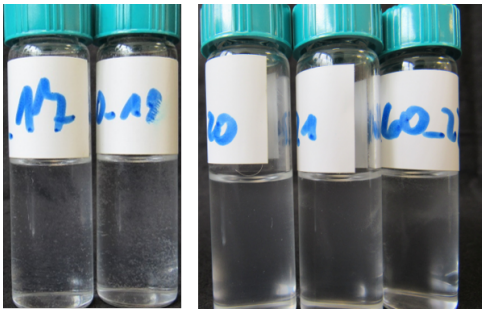

Fig. S 4 PMA/TTAB complexes. (From left: 245 mM TTAB + 1/2 mM PMA, 499 mM TTAB + 1/2/5 mM PMA.

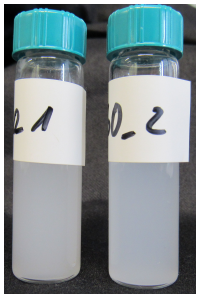

Fig. S 5 PAA/TTAB complexes. (From left: 30 mM PAA + 14/7 mM TTAB).

The picture Fig. S5 refers to a polymer excess sample but yields in the same precipitation for mixtures of 250 mM TTAB + 1/2 or 3 mM TTAB and 499 mM TTAB +1/2/3 or 8 mM TTAB. The PAA solution was previously adjusted to a pD of 8.5 by adding an appropiate NaOH solution to ensure a similar ionisation.

3 Rheology

The full shear flow-curves with the according fits are shown in Fig. S6, S7, S8.

The corresponding set of parameters determined via the Carreau−Yasuda fit (Equ. 1) are summarized in Table S1,S2, S3.

The relaxation time (Fig. S9) was also determined via the critical shear rate, where two linear fits (one in the Newtonian and one in the shear thinning regime) were performed and the intersect of both results in similar critical shear rates/relaxation times.

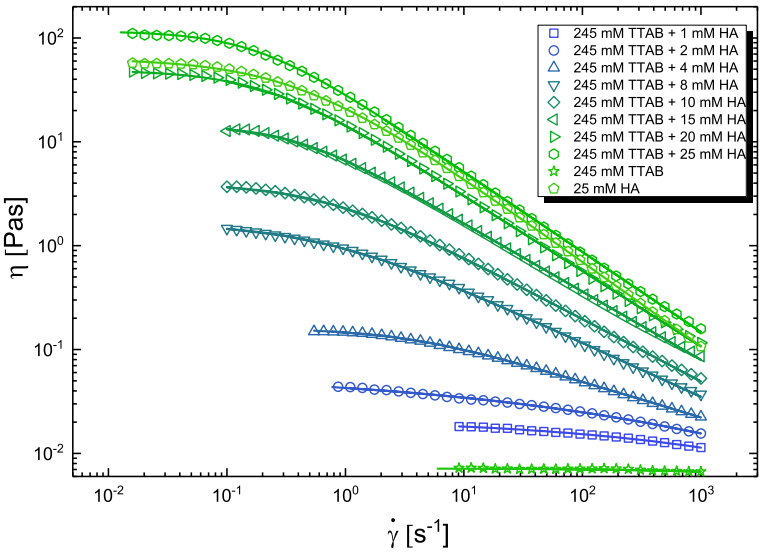

Fig. S 6 Viscosity as a function of the shear rate for different concentrations of HA in 245 mM TTAB mixtures (all samples at 25 °C and in 160 mM NaBr in D_2O). The solid lines are the fits according to the Carreau-Yasuda model (Eq.1).

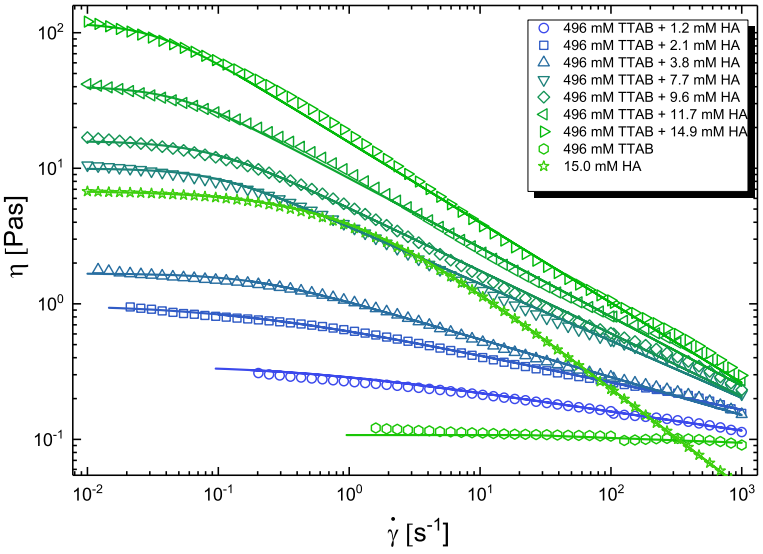

Fig. S 7 Viscosity as a function of the shear rate for different concentrations of HA in 496 mM TTAB (all samples at 25 °C and in 160 mM NaBr in D_2O). The solid lines are the fits according to the Carreau-Yasuda model (Eq.1).

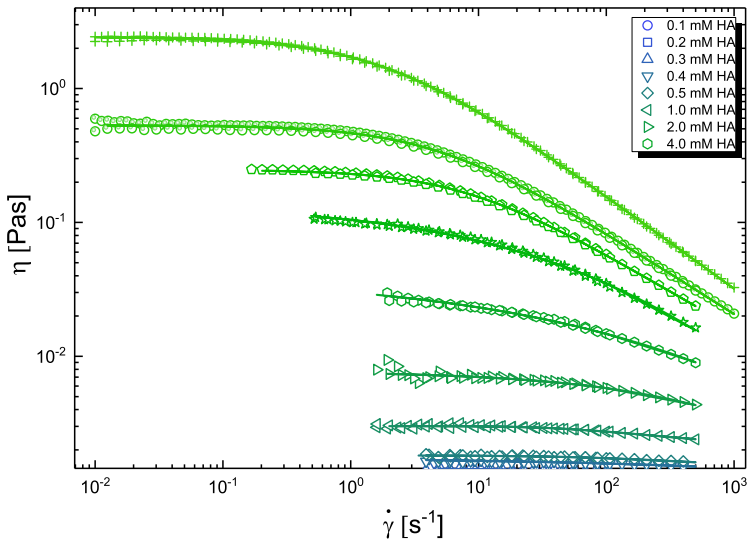

Fig. S 8 Viscosity as a function of the shear rate for different concentrations of HA, for pure HA solutions (all samples at 25 °C and in 160 mM NaBr in D_2O). The solid lines are the fits according to the Carreau-Yasuda model (Eq.1).

Table S 1 Fit parameter according to the Carreau-Yasuda fit performed on shear flow data.

c(HA) [mM]	τ	n	a	η_0 [mPas]	η_{spec}
245 mM TTAB/HA samples					
1	0	0.52	0.32	21.46	2
2	0	0.39	0.22	60.87	7.5
3.9	0.3	0.65	1.03	159.05	21.22
7.8	1.56	0.48	0.82	1646.9	229.06
10.4	1.48	0.4	0.99	3974.3	554.18
14.7	2.72	0.34	1.28	14478	2021.46
19.5	4.57	0.27	1.06	49035	6848.8
0	0	0.84	0.6	7.16	0

Table S 2 Fit parameter according to the Carreau-Yasuda fit performed on shear flow data.

c(HA) [mM]	τ	n	a	η_0 [mPas]	η_{spec}
496 mM TTAB/HA samples					
1.2	2.48	0.86	0.77	350.81	2.24
2.1	6.79	0.8	0.68	989.47	8.14
3.8	5.43	0.72	1.4	1671.5	14.44
7.7	10.48	0.58	1.7	9953.3	90.96
9.6	12.2	0.54	1.53	16044	147.23
11.7	21.33	0.49	1.72	40175	370.17
14.9	30.98	0.41	1.82	118360	1092.5
0	0.04	0.96	8.11	108.24	0

Table S 3 Fit parameter according to the Carreau-Yasuda fit performed on shear flow data.

c(HA) [mM]	τ	n	a	η_0 [mPas]	η_{spec}
HA samples					
1	0.03	0.92	1.77	3.01	1.97
2.01	0.02	0.79	1.15	7.16	6.05
3.9	0	0.01	0.3	39.82	38.19
6.11	0	0.01	0.4	137.82	134.65
8.11	0.13	0.44	1.01	244.97	240.11
9.75	0.2	0.39	0.93	530.97	521.61
13.43	0.51	0.31	0.88	2424.1	2384.93

Further oscillating measurements were performed (Fig. S11-13). Before each measurement a amplitude sweep was conducted to reassure being in the linear viscous region (Fig. S10) for the frequency sweep.

The crossover point (Fig. S14) is determined as the frequency where the loss and storage modulus equals. This frequency can be directly converted in an macroscopic relaxation time included in Fig. 4.

The Rheo-SANS experiments were performed just in radial set-up, which means, that the neutron beam hits perpendicular to the alignment/shear flow. A cup/bob geometry of titanium was used to be transparent to neutrons. The determination of the order parameter bases on a second-order Legendre polynomial as described in.[1]

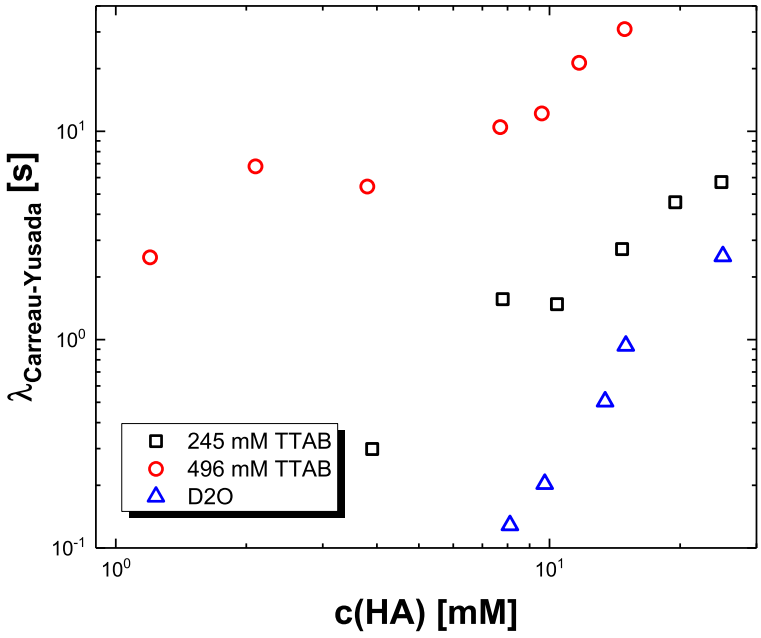

Fig. S 9 Relaxation times extracted from fits according to Eq. 1.

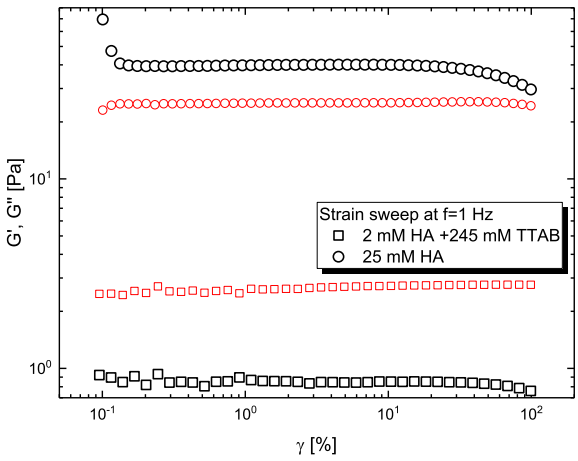

Fig. S 10 Loss (red) and storage modulus (black) of HA/245 mM TTAB samples at different amplitudes at a fixed frequency of 1 Hz for a HA gel and more liquid like sample.

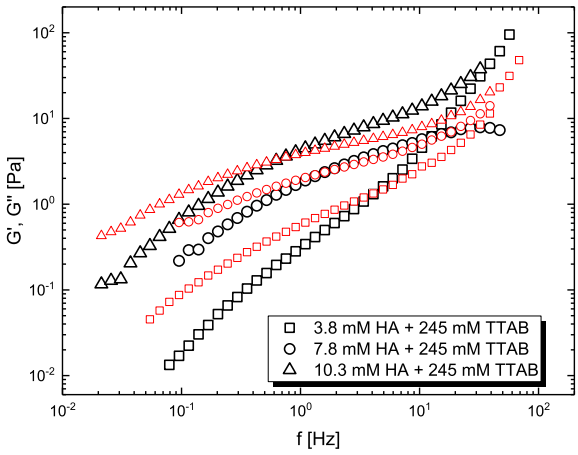

Fig. S 11 Loss (red) and storage modulus (black) of HA/245 mM TTAB samples at different frequencies.

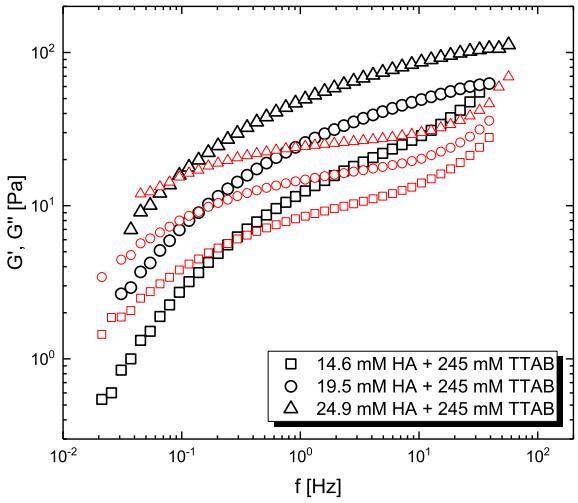

Fig. S 12 Loss (red) and storage modulus (black) of HA/245 mM TTAB samples at different frequencies.

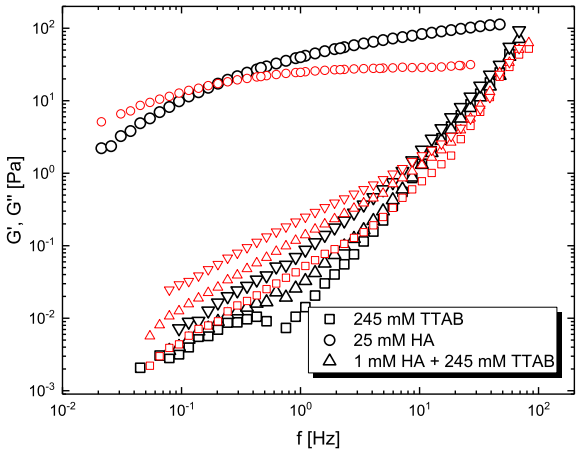

Fig. S 13 Loss (red) and storage modulus (black) of HA/245 mM TTAB samples at different frequencies.

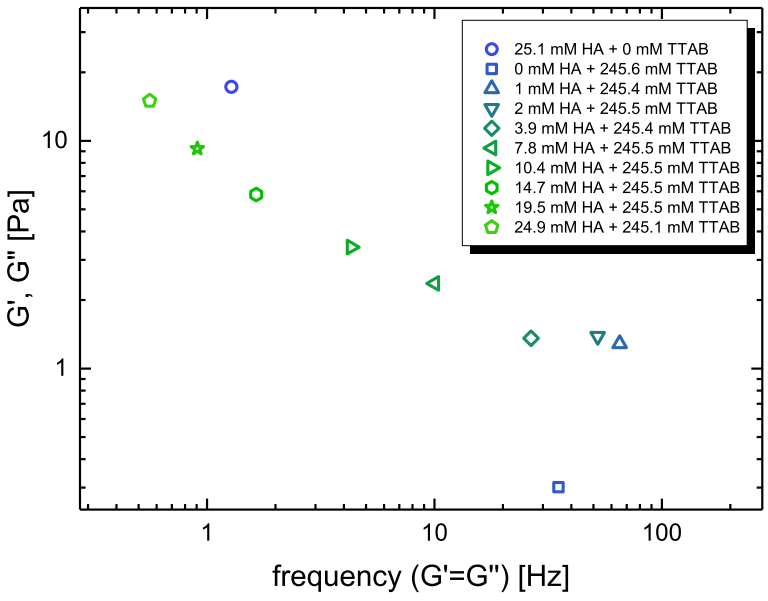

Fig. S 14 Crossover point of different HA/245 mM TTAB mixtures.

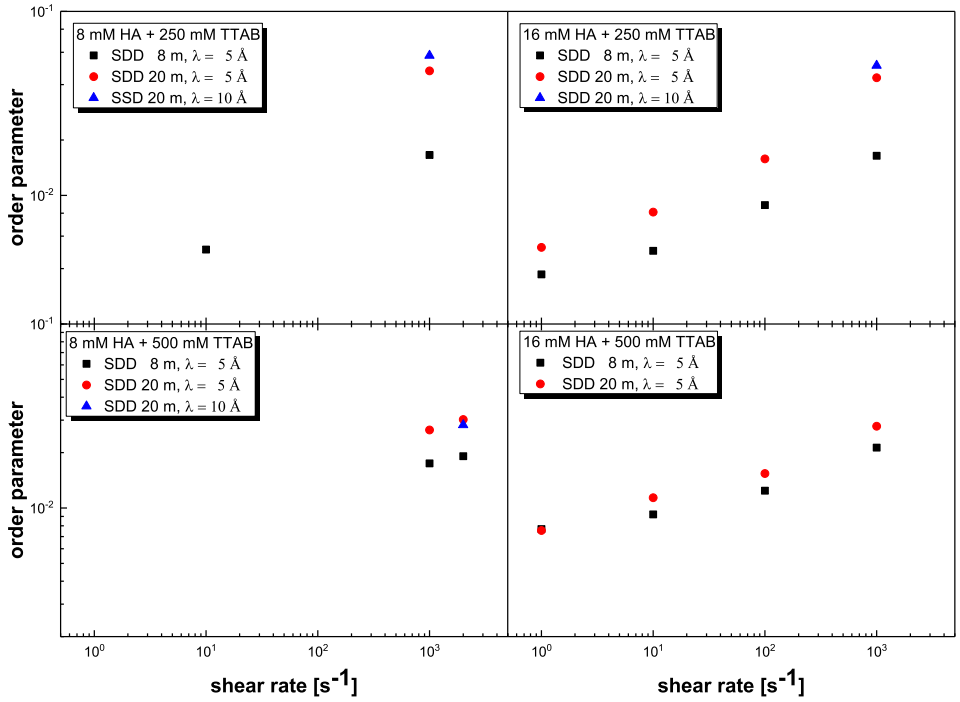

Fig. S 15 Order parameter versus shear rate for different HA/TTAB mixtures and different sample-to-detector-distances (SDD).

$$\langle P_2(\cos\varphi)\rangle = \frac{\int_0^\pi I(Q,\varphi)P_2(\cos\varphi)\sin\varphi d\varphi}{\int_0^\pi I(Q,\varphi)\sin\varphi d\varphi} \tag{1}$$

The data were obtained at the KWS 2 in Garchingen in Munich, Germany.

4 Static Light Scattering

For the characterization of the pure HA (see Fig. S16) and to assure the manufacturer's data, the MW and R_g were determined in 160 mM NaBr D_2O by means of static light scattering. For this purpose also the refractive index increment (dn/dc) was determined to be $0.138\,\mathrm{mL\,g^{-1}}$ by use of a differential refractometer (Scan-Ref Monocolor, NTF GmbH, Germany) after extensive dialysis to establish the Donnan equilibrium.[2] All experiments were carried out at 25 °C.

The light scattering experiments were performed three times: Directly

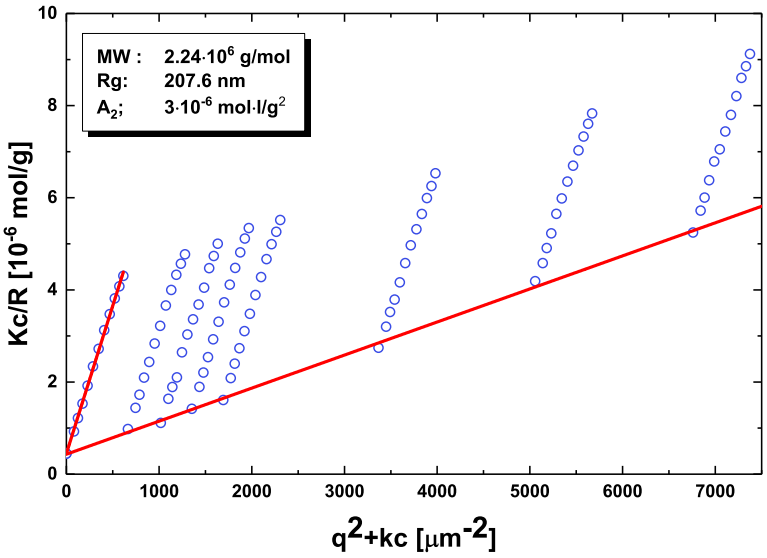

Fig. S 16 Zimm plot of pure HA in 160 mM NaBr in D_2O (k=30 l/g).

after the SANS-study, 1 and 6 months later. The data showed no significant alteration due to sedimentation or ageing. The Fig. S17 shows the absolute intensities for samples in 245 mM TTAB received in static light scattering experiments. The according SLS intensities for samples in 496 mM TTAB are summarized in Fig. S18.

According to Fukada,[3] the total persistence length of HA can be deduced from the slope of a KC/I vs Q^2 plot so that:

$$L_l = \frac{6m}{b} \frac{d[\frac{KC}{I(Q)}]}{dQ^2} \tag{2}$$

where m the mass and respectively b the length of the monomeric unit describes. Results of Applying Eq. 2 for the given SLS data are shown in Fig. S19.

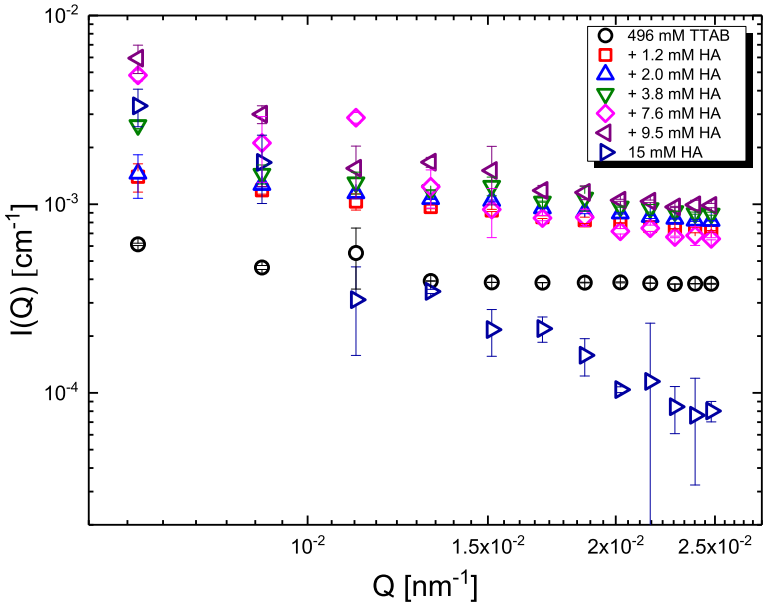

Fig. S 17 Static light scattering data from HA/TTAB complexes in 245 mM TTAB in 160 mM NaBr in D_2O.

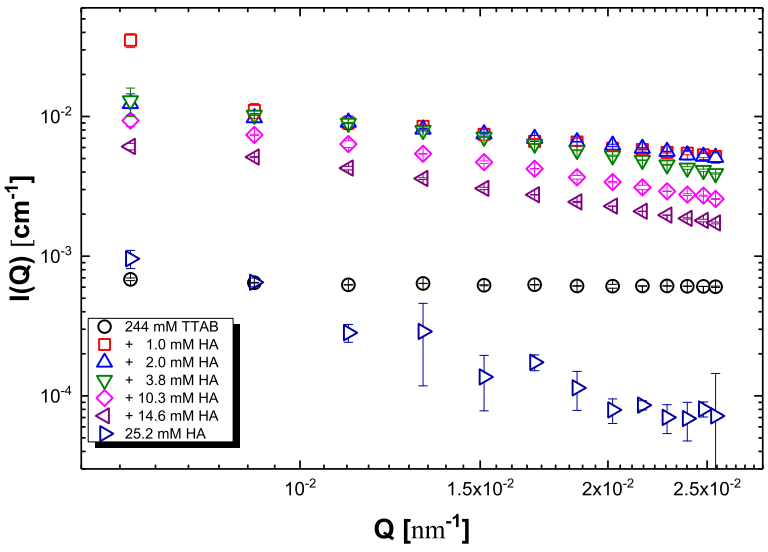

Fig. S 18 Static light scattering data from HA/TTAB complexes in 496 mM TTAB in 160 mM NaBr in D_2O.

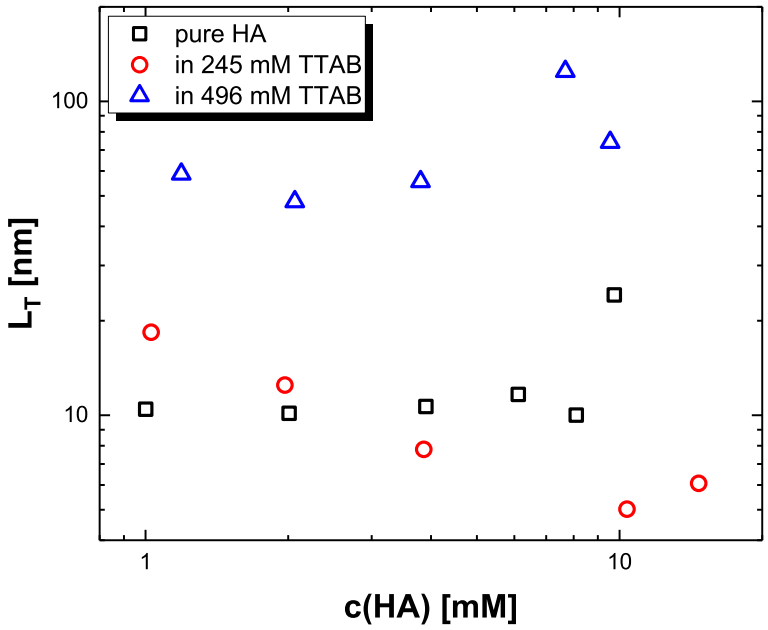

Fig. S 19 Estimation of the total persistence length based on the light scattering experiment and Eq. 2.

5 Dynamic light scattering (DLS)

The dynamic light scattering was performed on the samples of 245 mM TTAB and different amounts of HA. For all probes a set of 6 angles (40-120°) were measured (Fig. S20). The measured intensity autocorrelation function $g^{(2)}$ is related to the field autocorrelation function $g^{(1)}$ by the Siegert relation: $g^{(2)} = 1 + B\left|g^{(1)}\right|^2$. The analysis were performed considering a bimodal stretched exponential fit according to:

$$g(q,t)^{(1)} = BKG + A_{fast} exp\left(-(t/\tau_{fast})^{\beta_{fast}}\right) + A_{slow} exp\left(-(t/\tau_{slow})^{\beta_{slow}}\right) \quad (3)$$

From the fit parameter $\tau_{fast}, \tau_{slow}, \beta_{slow}, \beta_{fast}$ a mean decay time $< \tau >= \tau/\beta\Gamma(\beta)$, where Γ the gamma function is, was calculated and the slow mode $< \tau_{slow} >$ was compared with the relaxation time determined via rheology (Fig. 4). For the discussion of a more macroscopic view, just the correlation

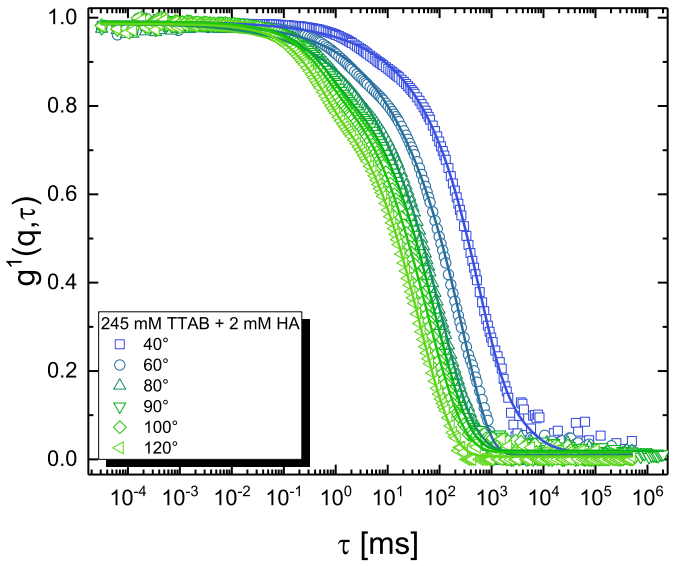

Fig. S 20 Example of the data treatment of the dynamic light scattering. Here all measured angles of a 245mM TTAB and 2 mM HA mixture in in 160 mM NaBr in D_2O are shown.

functions and the fit parameters thereof at an angle of 40 degrees were considered for this paper as they are shown in Fig. S21. Consequently the relaxation time gained in the dynamic light scattering should be considered as apparent values.

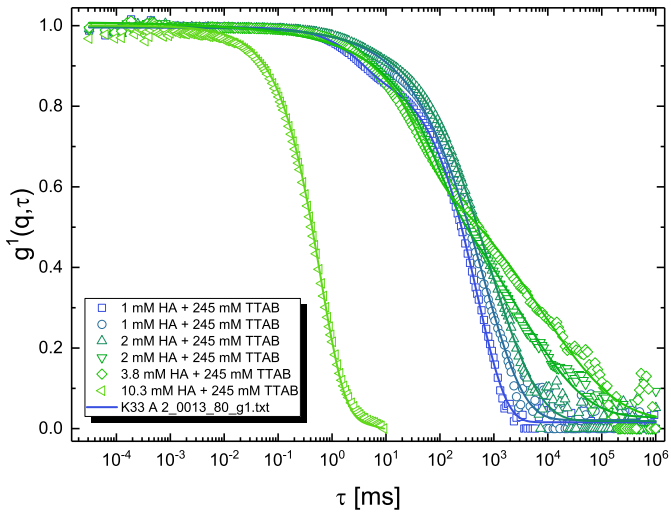

Fig. S 21 Autocorrelation function of HA/245 mM TTAB mixtures at 40°.

6 SANS (Small angle neutron scattering)

For modelling the scattering of the micelles a form factor

$$P_{\text{Ellipsoid}}(Q) = \left\langle F^2(Q,\mu)\right\rangle = \int_0^1 \left[F(Q,\mu)\right]^2 d\mu \tag{4}$$

with $\mu = \cos\alpha$ of a biaxial core-shell ellipsoid (rotational ellipsoid with the angle α between rotation axis and the scattering vector) was applied, where $F(Q,\mu)$ is the scattering amplitude as given by:

$$F(Q,\mu) = (\eta_c - \eta_{sh})V_c\left[\frac{3j_1(x_c)}{x_c}\right] + (\eta_{sh} - \eta_{sol})V_t\left[\frac{3j_1(x_t)}{x_t}\right] \tag{5}$$

Here SLD is the scattering length density for core, shell and solvent, respectively, $j_1(x)$ the first-order Bessel function for a regular sphere given as: $j_1(x) = \frac{\sin(x)-x\cos(x)}{x^2}$, the core volume $V = \frac{4}{3}\pi AB^2$ the shell volume $V_{\text{shell}} = V_{\text{total}} - V_{\text{core}}$ with the total volume $V_{\text{total}} = 4/3\pi(A+T)(B+T)^2$, and axis $x_c = Q\sqrt{A^2\mu^2 + B^2(1-\mu^2)}$, $x_t = Q\sqrt{(A+T)^2\mu^2 + (B+T)^2(1-\mu^2)}$ are used.[4] Due to the high concentration A was considered as polydisperse and following a lognormal distribution with $pdf(x,\mu,pdi) = \frac{1}{xpdi\sqrt{2\pi}} exp\left[-\frac{(ln(X)-ln(\mu))^2}{2pdi^2}\right]$, where pdf is the probability density function and pdi the polydispersity. The used

Table S 4 Scattering length densities used in this work.

name	formula	SLD/$10^{10} cm^{-2}$	Volume/nm^3
Solvent	160 mM NaBr in D_2O	6.307	
Core / tail	$C_{14}H_{29}$	-0.520	0.405
Dry shell/ head	$N^+C_3H_9$	-0.304	0.109

SLDs are summarized in Table S4.

The degree of solvent in the micelle head group shell is calculated as follows. A theoretical shell volume $V_{\text{theorshell}}$ is given by the volume ratio of the head to tail of the surfactant molecule $V_{\text{head}}/V_{\text{tail}}$ times the volume of the core resulting of the fit $V_{\text{theorshell}}$. The hydration ($\Phi_{\text{waterintheshell}}$) is the comparison between theoretical shell volume and the volume of the shell resulting of the fit V_{shellFit}.

$$\begin{aligned} V_{\text{theorshell}} &= V_{\text{coreFit}} \frac{V_{\text{head}}}{V_{\text{tail}}} \\ \Phi_{\text{waterintheshell}} &= \frac{(V_{\text{shellFit}} - V_{\text{theorshell}})}{V_{\text{shellFit}}} \end{aligned} \tag{6}$$

Hence the SLD of the shell can be calculated via $\Phi_{\text{waterintheshell}} SLD_{Solvent}(1-\Phi_{\text{waterintheshell}}) + (1-\Phi_{\text{waterintheshell}}) SLD_{N^+C_3H_9}$. The structure factor $S_{HardSphere}(Q)$ describes a pair interaction potential $U(r)$ which goes to infinity if a certain radius r is undershot so that the spheres can't inter penetrate.

$$\frac{U(r)}{k_B T} = \begin{cases} \infty & \text{for} \quad 0 < r < \sigma \\ 0 & \text{for} \quad r > \sigma \end{cases} \tag{7}$$

The hard sphere structure factor is depending on an effective repulsion radius R_{HS} and volume fraction f_p so that the mathematical expression is:

$$S_{HS}(Q, R_{HS}, f_p) = \frac{1}{1 + 24 f_p \frac{G(Q, R_{HS}, f_p)}{Q, R_{HS}}} \tag{8}$$

where

$$
\begin{aligned}
\alpha &= \frac{(1+2f_p)^2}{(1-f_p)^4} \\
\beta &= -6f_p\frac{f_p\alpha}{2} \\
A &= 2(R_{HS}+HYD)Q \\
G(Q) &= \alpha\frac{\sin A - A\cos A}{A^2} \\
&\quad + \beta\frac{2A\sin A - (2-A^2)\cos A - 2}{A^3} \\
&\quad + \gamma\frac{-A^4\cos A + [(3A^2-6)\cos A + (A^3-6A)\sin A + 6]}{A^5}
\end{aligned}
\tag{9}
$$

the f_p is here determined as the volume fraction of TTAB (Φ_{TTAB}) multiplied by the increasing volume due to a hydration shell of pure water molecues coordinated around the micelle (HYD) of $0.2\,\mathrm{nm}$ minus the volume faction of TTAB bound in the fractal so that:

$$
f_p = (\Phi_{TTAB} - \chi_{bound})(\frac{R_{HS}+HYD}{R_{HS}})^3 \tag{10}
$$

The unique behaviour of HA in an excess of oppositely charged surfactants is further underlined, comparing it to SANS data of pure HA solutions where a fractal dimension of 2.7-3 is dominating (Fig. S 22).

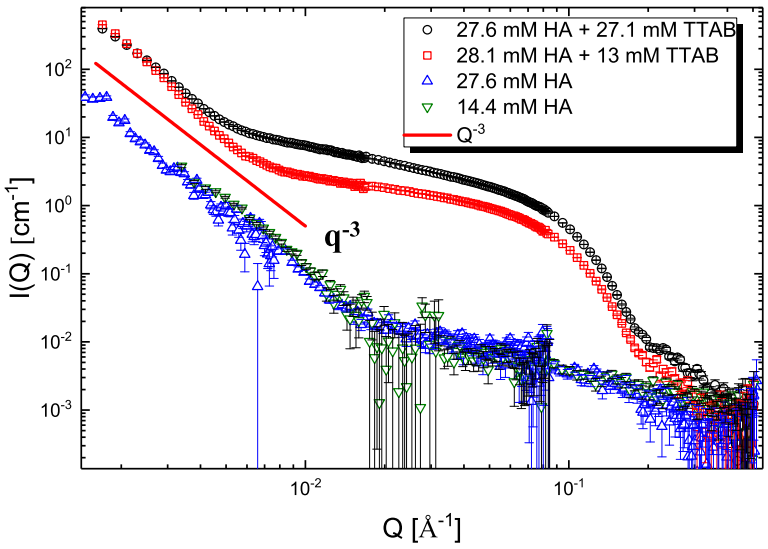

Fig. S 22 SANS intensities of pure HA in 160 mM NaBr in D_2O and of HA/TTAB mixtures wherein HA is in excess.

7 Comparison SANS/SLS results

The precise values concerning the contrast (among others the scattering length density (SANS) and refractive index increment (SLS)) are not easily accessible for the formed complexes. Therefore differences are arising if values like MW are determined. As Fig. S23 shows, an offset of around a factor 2 is given by assuming the total concentration (c(HA)+c(TTAB)) contributes to the forward scattering.

Considering that just the aggregates (c(HA) + c(χ_{bound})) are visible the offset is a factor of 0.9. This offset might be due to the fact that χ_{bound} can't directly be converted in the scattering contribution for SLS. The case for samples in 496 mM is the same (Fig. S24).

However, the most important statement of the comparison is, that the data is self consistent and yields in the same qualitative characteristics of the systems. As mentioned before, the offsets have had to be expected and not avoidable due to the nature of the system and technique.

The aggregation numbers according to the calculated MW for samples in 496 mM TTAB are shown inn Fig. S25. For the calculation of N_{Agg} both

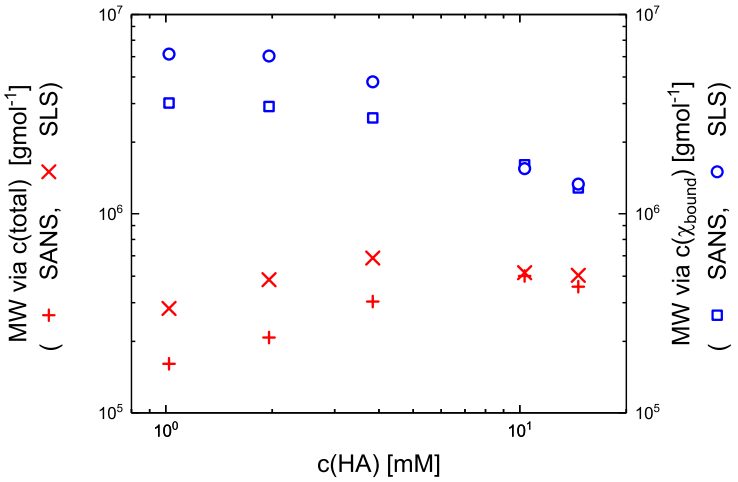

Fig. S 23 Direct comparison of the results for the MW according to the total concentration (left axis) and on χ_{bound} (right axis) for samples in 245 mM TTAB.

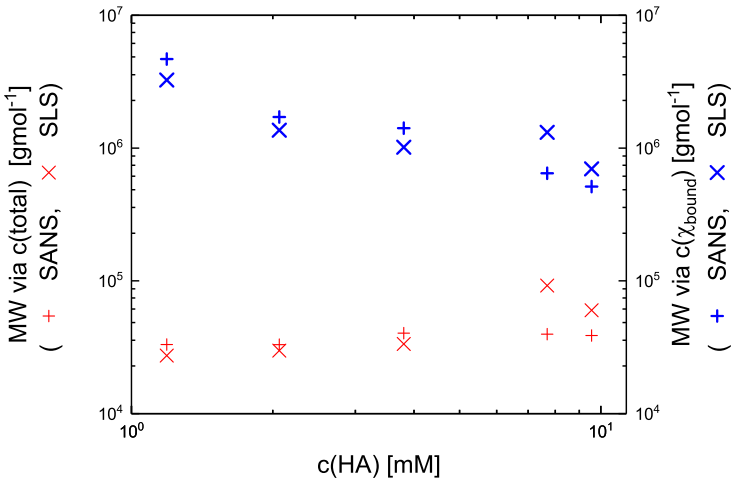

Fig. S 24 Direct comparison of the results for the MW according to the total concentration (left axis) and on χ_{bound} (right axis) for samples in 496 mM TTAB.

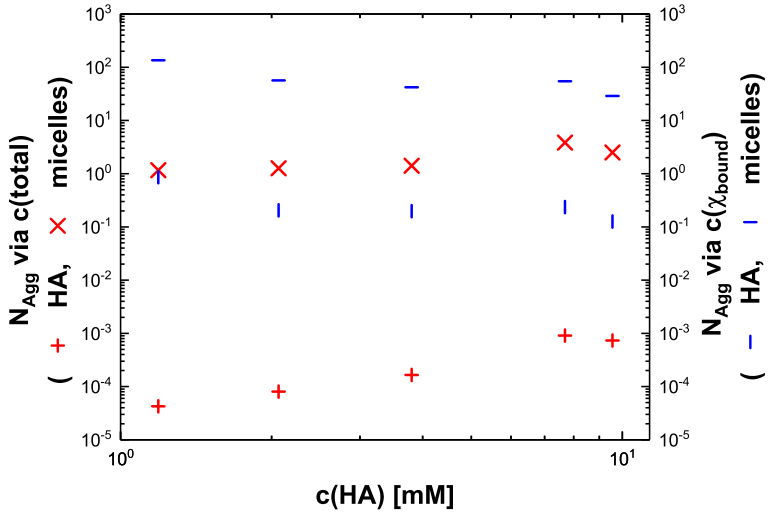

Fig. S 25 Aggregation number for HA/496 mM TTAB samples according to a total concentration and to χ_{bound}.

MW, the one based on the total concentration and of the estimated concentration of the aggregates, were used. According to the stoichiometric ratio the aggregation number was calculated as follows:

$$N_{Agg}\,(HA) = \frac{\frac{c(HA)}{c(total)} MW_{determined}}{MW_{HAchain}} \tag{11}$$

The aggregation number of TTAB was calculated accordingly.

References

[1] M. Muthig, S. Prévost, R. Orglmeister and M. Gradzielski, *J Appl Cryst*, 2013, **46**, 1187–1195.

[2] K. Takashima, K. Nakae, M. Shibata and H. Yamakawa, *Macromolecules*, 1974, **7**, 641–649.

[3] K. Fukada, E. Suzuki and T. Seimiya, *Langmuir*, 1999, **15**, 4217–4221.

[4] L. Chiappisi, D. Li, N. J. Wagner and M. Gradzielski, *The Journal of Chemical Thermodynamics*, 2014, **68**, 48–52.